ADVANCED MATERIALS

[26] A. B. Murray, G. Reydellet, *J. Coast. Res.* **2001**, *17*, 517.
[27] A. Pockels, *Nature* **1892**, *46*, 437.
[28] N. Lu, M. Gleiche, J. Zheng, S. Lenhert, B. Xu, L. F. Chi, H. Fuchs, *Adv. Mater.* **2002**, *14*, 1812.
[29] Y. Xia, X.-M. Zhao, G. M. Whitesides, *Microelectron. Eng.* **1996**, *32*, 255.
[30] D. Wang, S. G. Thomas, K. L. Wang, *Appl. Phys. Lett.* **1997**, *70*, 1593.
[31] P. M. St. John, H. G. Craighead, *Appl. Phys. Lett.* **1996**, *68*, 1022.
[32] J. Zheng, Z. Zhu, H. Chen, Z. Liu, *Langmuir* **2000**, *16*, 4409.
[33] J. Kim, Y. Oh, H. Lee, Y. Shin, S. Park, *Jpn. J. Appl. Phys., Part 1* **1998**, *37*, 7148.
[34] D. W. Carr, M. J. Lercel, C. S. Whelan, H. G. Craighead, K. Seshadri, D. L. Allara, *J. Vac. Sci. Technol. A* **1997**, *15*, 1446.
[35] M. Geissler, H. Schmid, A. Bietsch, B. Michel, E. Delamarche, *Langmuir* **2002**, *18*, 2374.
[36] Curtis, C. Wilkinson, *Biomaterials* **1997**, *18*, 1573.
[37] L. Feng, S. Li, Y. Li, H. Li, L. Zhang, J. Zhai, Y. Song, B. Liu, L. Jiang, D. Zhu, *Adv. Mater.* **2002**, *14*, 1857.

Efficient Organic Electrophosphorescent White-Light-Emitting Device with a Triple Doped Emissive Layer**

By *Brian W. D'Andrade*, *Russell J. Holmes*, and *Stephen R. Forrest**

The use of organic light-emitting devices (OLEDs) for general purpose illumination is being given careful consideration, since OLED power efficiency is now approaching that of incandescent bulbs.[1] The ultimate goal is to demonstrate a device that has an efficiency exceeding that of fluorescent bulbs, which are among the most power-efficient illumination sources available. Here, we discuss three principle means for achieving a high external power efficiency[2] (η_p) white OLED (WOLED): using thin layers for low voltage operation, efficiently confining charge and excitons within the emissive layer (EML), and using direct triplet exciton formation on a blue dopant with a high quantum yield. Additionally, we examine the energy transfer process between dopants, and investigate the dependence of outcoupling efficiency on absorption and reflection losses. A WOLED that combines these strategies, resulting in power efficiencies equal to or exceeding those of the best incandescent light sources, is also described. The devices have a peak total power efficiency of (42 ± 4) lm W^{-1} at low intensities, falling to (14 ± 2) lm W^{-1} at a drive current of 10 mA cm^{-2} (corresponding to 0.8 lm cm^{-2} for an isotropic illumination source). The Commission Internationale de L'Eclairage[3] (CIE) coordinates shift from (0.43,45) at 0.1 mA cm^{-2} to (0.38,0.45) at 10 mA cm^{-2}, and a color rendering index[4] (CRI) = 80 is obtained.

The electrophosphorescent device employs an EML containing three metallorganic phosphors: 2 wt.-% iridium(III) bis(2-phenyl quinolyl-N,C$^{2'}$) acetylacetonate (PQIr) providing red emission, 0.5 wt.-% *fac*-tris(2-phenylpyridine) iridium ($Ir(ppy)_3$) for green emission, and 20 wt.-% bis(4′,6′-difluorophenylpyridinato)tetrakis(1-pyrazolyl)borate (FIr6) for blue emission, all simultaneously co-doped into a wide energy gap *p*-bis(triphenylsilyly)benzene (UGH2) host. It has previously been shown that blue OLEDs employing FIr6 in the inert host UGH2 results in direct charge injection and triplet exciton formation on FIr6. Additionally, FIr6 transports both holes and electrons.[5] The process of direct triplet exciton formation results in high luminance efficiency blue and white electrophosphorescence, since the elimination of host–guest energy transfer avoids exchange energy losses common to earlier red, green, and blue electrophosphorescent OLEDs.[6]

The external quantum efficiency of a WOLED[2] (η_{ext}) is significantly affected by the thicknesses of the EML and electron transport layer (ETL).[7] Inefficient charge and exciton confinement severely reduces η_{ext} when the EML thickness is < 5 nm,[7] and additional reductions in efficiency are incurred when the ETL thickness is < 25 nm due to exciton quenching at the metal cathode. The optimized device in Figure 1 (fabricated as described in the Experimental section) effectively balances the competing effects of lower operating voltage and reduced quantum efficiency of thin devices. The current density versus voltage (*J*–*V*) characteristics are shown in the inset of Figure 2. The slope of the *J*–*V* curve decreases significantly above 4 V, as observed previously for thin p–i–n OLEDs.[8] This is attributed to space charge effects at high current densities (> 1 mA cm^{-2}).

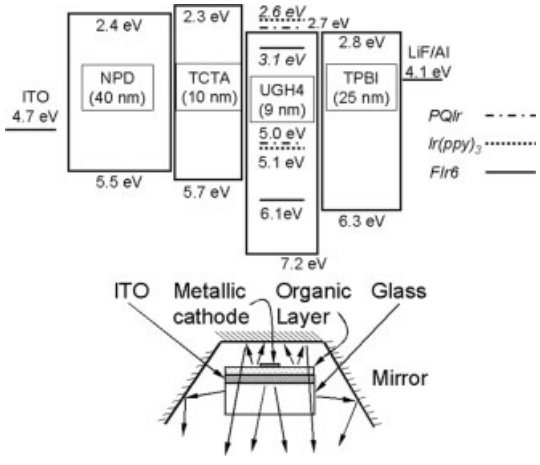

Figure 1. Top: Proposed energy level diagram of a white organic light-emitting device (WOLED) showing the highest occupied and lowest unoccupied molecular orbital energies relative to vacuum, the thicknesses and the acronyms for the constituents used. Bottom: Example of a WOLED lamp fixture.

[*] Prof. S. R. Forrest, B. W. D'Andrade, R. J. Holmes
Department of Electrical Engineering, Princeton University
Princeton, NJ 08544 (USA)
E-mail: forrest@Princeton.EDU

[**] The authors thank the Universal Display Corporation for their partial support of this work.

  DOI: 10.1002/adma.200306670

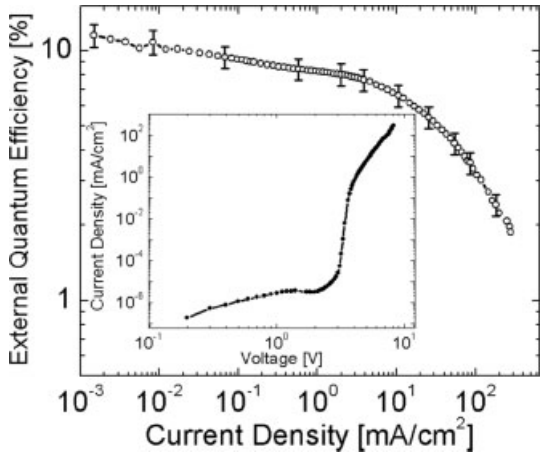

Figure 2. External quantum efficiency versus current density of the triple doped white organic light-emitting device (WOLED). Inset: Current density versus voltage characteristics of the WOLED.

Measurable emission is observed at 3.3 V, which is near the estimated 3.0 V necessary to directly generate a blue-emitting triplet exciton on a FIr6 dopant molecule, assuming near resonant injection of holes in 4,4′,4″-tri(*N*-carbazolyl)triphenylamine (TCTA)[9] into the highest occupied molecular orbital (HOMO), and electrons in 1,3,5-tris(*N*-phenylbenzimidazol-2-yl)benzene (TPBI)[10] into the lowest unoccupied molecular orbital (LUMO) of FIr6. The voltage required to excite green and red emission from $Ir(ppy)_3$ and PQIr, respectively, is < 3.0 V, so it is expected that the emission color will shift with increasing voltage, as observed (see inset Fig. 3, where normalized intensity is plotted against wavelength). The CIE coordinates of (0.43,0.45) at 0.1 mA cm^{-2} blue-shift to (0.38,0.45) at 10 mA cm^{-2}, with CRI = 80. The luminance is 1000 cd m^{-2} at ~5 V, which is the lowest operating voltage reported for a WOLED emitting at such a high luminance,[1,11] and is due to the use of thin, multiply doped layers along with near resonant charge injection followed by direct triplet formation on FIr6.

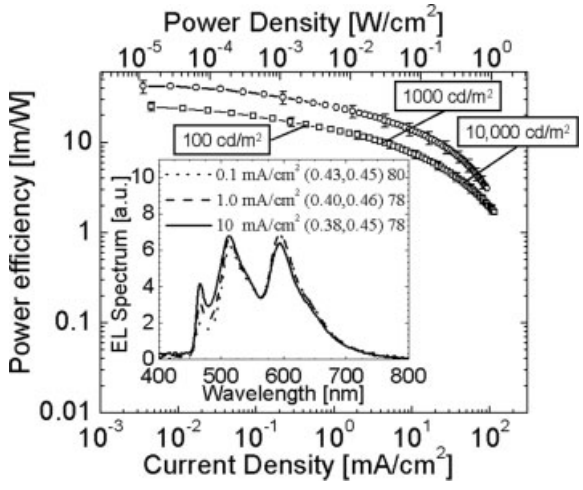

Figure 3. Lighting (circle) and display-relevant (square) power efficiencies versus current (lower abscissa) and power density (upper abscissa). The 5 mm^2 WOLEDs emit a maximum optical power of 2.8 lm cm^{-2}, and have a maximum total power efficiency of $\eta_t = 42$ lm W^{-1}. Inset: Normalized electroluminescence spectra of WOLED emission at various current densities. Also shown are the CIE coordinates, followed by the color rendering index value at each current density (indicated as (*X*,*Y*) CRI). Note the slight blue-shift as current density is increased.

The effectiveness of charge confinement relies on differences in LUMO and HOMO levels between the EML and the adjacent layers. As in Figure 1, the LUMO of the TCTA is at least 0.3 eV above that of the dopants and host, thus preventing electron leakage from the EML. In addition, the 0.2 eV energy barrier between the HOMO of FIr6 at 6.1 eV and TPBI at 6.3 eV acts as an efficient barrier to hole transport across the EML/ETL interface. Exciton diffusion from the EML towards the electron and hole transport layers is also prevented by employing materials with energy gaps greater than that of the blue dopant. Here, TCTA and TPBI have energy gaps of 3.4 eV and 3.5 eV, respectively, which are > 0.3 eV higher than that of FIr6. These barriers improve the charge balance and hence the recombination efficiency within the 9 nm thick EML, leading to improvement in η_{ext}.

Given these considerations, an optimized WOLED has a maximum forward viewing $\eta_p = (26 \pm 3)$ lm W^{-1} at low luminosity, decreasing to $\eta_p = (11 \pm 1)$ lm W^{-1} at 1000 cd m^{-2} with CRI > 75 (see Fig. 3, squares). The majority of excitons are generated by trapping on FIr6, and then subsequently transferred to the green and red dopants. Hence, the quantum efficiency of the blue dopant limits that of the entire device. Indeed, we obtain a maximum $\eta_{ext} = (12 \pm 1)$ % at low currents, decreasing to (6.7 ± 0.7) % at 10 mA cm^{-2} (see Fig. 2), consistent with previously reported FIr6-based OLEDs.[5]

To understand the energy transfer mechanisms between the phosphorescent dopants, we examine the photoluminescence transient decay in thin films of UGH2 doped at 20 wt.-% with FIr6, and of the triple doped EML. Given an energy gap of 4.4 eV (shown in Fig. 1), the UGH2 host does not significantly absorb at the excitation wavelength (337 nm), so energy transfer from the host is not expected to occur. The optical density of FIr6 in the triple doped film is at least ten times higher than either of the other dopants, due to its significantly higher concentration (20 % versus 0.5 % for green and 2 % for red). Therefore, the transfer processes originating from the excitation of FIr6 to the various dopants that result in broad spectral emission can be schematically depicted as in Figure 4, inset. Energy transfer from FIr6 to both $Ir(ppy)_3$ and PQIr is shown as dotted lines; radiative energy transfer from $Ir(ppy)_3$ to PQIr is possible (open arrow), but the low concentration of both species makes this process unlikely, and radiative relaxation to the ground state is shown as solid lines.

The time rate of decay of FIr6, $Ir(ppy)_3$, and PQIr in the triple doped film were taken from their peak emissions centered at $\lambda = 460$, 510, and 600 nm, respectively. Figure 4 shows that the lifetime of FIr6 decreases from $\tau = (1.60 \pm 0.01)$ μs in a UGH2:FIr6 film, to 0.75 μs in the triple doped system.

ADVANCED MATERIALS

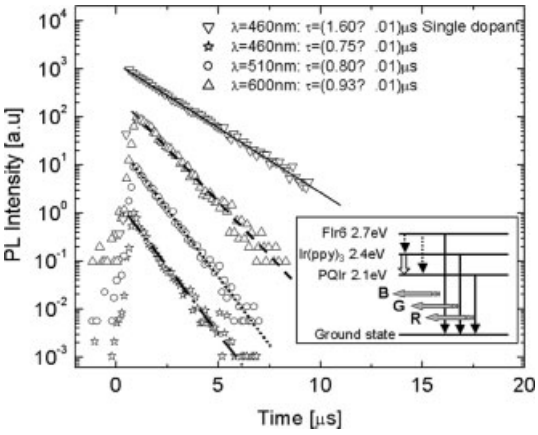

Figure 4. Photoluminescent decay transients for FIr6, $Ir(ppy)_3$ and PQIr co-doped into an UGH2 inert host, and for FIr6 doped into UGH2 (stars, circles, triangles, and inverted triangles, respectively). The lines are monoexponential fits to the data giving the rates noted in the upper right. Inset: Energy transfer pathways between FIr6, $Ir(ppy)_3$, and PQIr and the ground states. Dotted lines depict energy transfer between FIr6 and other dopants; the open arrow shows the unlikely transfer between $Ir(ppy)_3$ and PQIr, and solid lines show the radiative relaxation from the excited states of the dopants to the their respective ground states.

Previously measured lifetimes of $Ir(ppy)_3$[12] and PQIr[13] are $\tau = 0.8$ μs, and 2.0 μs. Indeed, we find that $\tau = (0.80 \pm 0.01)$ μs, and (0.93 ± 0.01) μs for peak emission at $\lambda = 510$ nm and 600 nm. Hence, the lifetime decrease in the triple doped film suggests that FIr6 emission is quenched primarily by energy transfer to the green and red dopants. The lifetime of $Ir(ppy)_3$ remained unchanged from previous reports,[12] which suggests that there is insignificant energy transfer from $Ir(ppy)_3$ to PQIr. The difference in the measured lifetimes of PQIr between that reported by Lamansky and co-workers[13] is due to the use of a microsecond flash lamp to measure the lifetime of PQIr (which can introduce errors in measuring sub-microsecond transients), instead of the picosecond streak camera used in this work.

In characterizing WOLEDs for white light displays, it is important to account for light waveguided in both the glass substrate and in the device and contact layers.[14,15] This waveguided light can exit from the sides of the substrate, or from the metal cathode surface (back) of the OLED, and is therefore lost for display applications. Unlike displays, efficient lamp fixtures can redirect light exiting from all surfaces into the space being illuminated. For example, the fixture in Figure 1 redirects light emitted from the sides and back of a small area WOLED into the forward direction. Hence, it is standard practice in the lighting industry[16] to state the total power efficiency (η_t) based on the total number of photons emitted, requiring measurement with an integrating sphere.[2] Figure 3, therefore, also shows η_t (circles) versus electrical power. We obtain $\eta_t = 42 \pm 4$ lm W^{-1} at low luminance intensity, decreasing to 10 ± 1 lm W^{-1} at 20 mA cm^{-2}. To obtain optical powers of ~800 lm typically used for room lighting applications,[16] an optimized device area of approximately 600 cm^2 is inferred from Figure 3. Using FIr6 as the blue dopant provides substantial gains in quantum efficiency over other blue dopants used in previous work.[11,17,18] A comparison between the performance of our structure and those previously reported is provided in Table 1.

When indium tin oxide (ITO) losses are ignored,[19] we find 19 % of the light is directly coupled out the front of the device, 34 % is waveguided between the glass–air and organic–air interfaces and exits from the substrate, and 48 % is waveguided in ITO (assuming typical values for the refractive indices of $n_{glass} = 1.5$, $n_{ITO} = 1.8$ and $n_{organic} = 1.7$, a substrate thickness $t = 0.1$ cm, and an average distance from the center of the device to the substrate side, $d = 1.5$ cm). However, when losses due to absorbed waveguided light in ITO (with an average absorption coefficient, α, over the visible of 2000 cm^{-1}) are considered, a smaller fraction of the 34 % waveguided light exits.

Quantitatively, for a particular emission angle, θ (defined as the angle between the direction of the light emitted in the organic layer and the substrate surface normal), a ray has m reflections before it exits the substrate and travels a distance, L, through ITO after each reflection. The total distance traveled through ITO is then:

$$m \times l = \frac{d}{t \times \tan\beta} \times \frac{a}{\cos\phi} \quad (1)$$

where

$$\phi = \sin^{-1}((n_{organic}/n_{ITO}) \sin\theta),$$

$$\beta = \sin^{-1}((n_{ITO}/n_{glass}) \sin\phi)$$

Table 1. Selected WOLED architectures with their corresponding performance characteristics. Where the color rendering index (CRI) is not reported, a maximum value is estimated from spectral data.

Architecture	η_{ext} [%] [a]	η_p [lm W^{-1}] [b]	CIE [c]	CRI	Refs.
Phosphorescent triple-doped emissive layer	12	26, 42	(0.43,0.45)	80	This work
Multilayer phosphorescent	12	10, 17	(0.35,0.36)	≤60	[1]
Phosphorescent excimer	6.4	12.2, 21	(0.36,0.44)	67	[11]
Multi-emissive phosphor doped layers	5.2	6.4, 11	(0.37,0.40)	83	[18]
Two doped and one neat emissive layers	–	1.93, 3.3	(0.35,0.34)	≤80	[23]
Doped blocking layers	–	1.39, 2.4	–	–	[24]
Multiple quantum wells	–	1.1, 1.9	(0.32,0.38)	≤80	[25]
Interlayer sequential energy transfer	0.5	0.35, 0.6	(0.33,0.33)	≤70	[26]
Hybrid polymer/inorganic	1.9	0.63, 1.1	(0.34,0.29)	≤70	[27]
Three neat emissive layers	0.7	0.5, 0.9	(0.31,0.41)	≤80	[28]
Triple doped polymer with vacuum deposited transport layers	–	0.83, 1.4	–	–	[29]

[a] Maximum reported forward viewing external quantum efficiency. [b] Maximum reported forward viewing external power efficiency is the first number. The second is the total external power efficiency. Where not reported, it is the maximum forward viewing external power efficiency multiplied by 1.7 that assumes a small area contact (see text). [c] Commission Internationale de l'Eclairage coordinates at 100 cd m^{-2}.

Hence, the fraction, f, of the total light exiting from the sides of the substrate is:

$$f = \int_{\theta_1}^{\theta_2} \sin\theta \times \exp(-\alpha m l)\, d\theta \quad (2)$$

Here, $\theta_1 = 36.0°$ and $\theta_2 = 61.9°$ are the critical angles for air–organic and glass–organic interfaces, respectively. From Equation 2, we calculate $f = 0.24$, so the total fraction of light outcoupled from both the front and sides of the substrate is 0.43, versus 0.19 outcoupled from the front surface alone. Since power efficiency is directly proportional to outcoupling efficiency, the ratio of the total power emitted from the device versus the power emitted from the front is given by $\eta_t/\eta_p = 0.43/0.19 = 2.3$, compared to 1.7 ± 0.2 obtained experimentally. This agreement suggests that η_t/η_p can be accounted for primarily by losses in ITO absorption, although several other factors such as interface roughness and non-ideal cathode metal reflectivity, can also reduce η_t.

For practical devices with an area > 600 cm^2, the small active area approximation used to derive Equations 1 and 2 suggests that a negligibly small fraction of the light will exit from the side of the substrate. Additionally, a large-area metal cathode will cause significant absorption losses (approximately 15 %[20] upon each reflection at the organic–metal interface). Therefore, efficiently outcoupling light in the forward or backward direction, or utilizing structures with highly reflective (> 95 %) metal, or thin (< 150 nm) ITO cathodes, is essential. Table 2 compares the area of five triple-doped WOLEDs using various outcoupling schemes, operating at 12 lm W^{-1}, and emitting a total of 800 lm. Note that the most effective outcoupling scheme employs shaped substrates that emit all locally generated light into the forward viewing direction.[21] In this case, 800 lm require a surface area of only 650 cm^2.

Table 2. Selected outcoupling schemes for a triple doped WOLED emitting a total of 800 lm and operating at 12 lm W^{-1}, which is comparable to an incandescent bulb.

Outcoupling scheme	F [a]	Area [cm^2] [b]	Refs.
Conventional WOLED	1.0	7100	This work
Top emitting	1.2	3200	[30]
Nanopatterning of glass substrate	1.5	1400	[31]
Microlens array	1.5	1400	[32]
Silica aerogels	1.8	750	[33]
Shaped substrates	1.9	650	[21]

[a] Factor of outcoupling efficiency improvement over conventional WOLED. [b] Active area of WOLED.

In conclusion, we have demonstrated a high efficiency WOLED with a thin electrophosphorescent triple doped host, and efficient exciton and charge confinement. Devices have $\eta_p = (14 \pm 1)$ lm W^{-1} at 10 mA cm^{-2}, a maximum $\eta_t = (42 \pm 4)$ lm W^{-1} and CIE coordinates that vary from (0.43,45) at 0.1 mA cm^{-2} to (0.38,0.45) at 10 mA cm^{-2}, with CRI = 80. The device emission color is effectively controlled by varying dopant concentrations. As in the case of recently reported deep-blue-emitting electrophosphorescent OLEDs,[5] high efficiency is obtained by direct triplet formation on the blue dopant by near-resonant charge transfer from nearby charge injection layers, thereby avoiding exchange energy losses incurred by energy transfer from a singlet exciton state in the host to a triplet state in the phosphor.

Experimental

Devices were grown on glass substrates pre-coated with an $a = 150$ nm thick layer of indium tin oxide (ITO) with a sheet resistance of 20 Ω/sq. Substrates were degreased with solvents and then cleaned by exposure for 5 min to an ultraviolet–ozone ambient. All organic layers were grown in succession without breaking vacuum ($\sim 1 \times 10^{-7}$ torr) and affixing a shadow mask, with either 1 mm diameter dots, or 5 mm^2 rectangular openings to define the cathode. Growth was completed in a nitrogen filled glove box with < 1 ppm water and oxygen. The device structure (see Fig. 1 for energy level scheme) consists of a 40 nm thick 4,4′-bis[*N*-(1-naphthyl)-*N*-phenyl-amino]biphenyl (NPD) hole transport layer, followed by a 10 nm thick layer of TCTA that confines excitons and electrons in the EML. The 9 nm thick white EML consists of a mixture of three electrophosphorescent dopants: 20 wt.-% FIr6, 0.5 wt.-% Ir(ppy)$_3$, and 2 wt.-% PQIr [13] co-doped into a UGH2 host. Finally, a 25 nm thick electron transporting and hole blocking layer consisting of TPBI was deposited. Cathodes consist of a 0.5 nm thick layer of LiF followed by a 50 nm thick layer of Al.

The HOMO energy for each material was measured using ultraviolet photoemission spectroscopy, except that of NPD, which is from Ref. [22]. The corresponding LUMO energy was estimated by adding the energy corresponding to the onset of absorption to the HOMO energy. This generally underestimates the carrier transport gap, although this underestimate is expected to be comparable for all of the organic materials used, allowing for a relative comparison of LUMO level positions relative to vacuum.

50 nm thick films of UGH2 doped at 20 wt.-% with FIr6 and of the triple doped EML were grown on quartz for optical transient measurements. These measurements were performed at 300 K, using a nitrogen laser emitting at $\lambda = 337$ nm with a 500 ps pulse, and a streak camera. Lifetimes were estimated from monoexponential fits to the data.

Received: December 23, 2003
Final version: February 9, 2004

[1] S. Tokito, T. Iijima, T. Tsuzuki, F. Sato, *Appl. Phys. Lett.* **2003**, *83*, 2459.
[2] S. R. Forrest, D. D. C. Bradley, M. E. Thompson, *Adv. Mater.* **2003**, *15*, 1043.
[3] *Colorimety*, Commission Internationale de L'éclairage (CIE), Paris **1986**.
[4] *Method of Measuring and Specifying Colour Rendering Properties of Light Sources*, Commission Internationale de L'Eclairage (CIE), Paris **1974**.
[5] R. J. Holmes, B. W. D'Andrade, X. Ren, M. E. Thompson, S. R. Forrest, *Appl. Phys. Lett.* **2003**, *83*, 3818.
[6] R. J. Holmes, S. R. Forrest, Y. J. Tung, R. C. Kwong, J. J. Brown, S. Garon, M. E. Thompson, *Appl. Phys. Lett.* **2003**, *82*, 2422.
[7] B. W. D'Andrade, S. R. Forrest, *J. Appl. Phys.* **2003**, *94*, 3101.
[8] M. Pfeiffer, S. R. Forrest, K. Leo, M. E. Thompson, *Adv. Mater.* **2002**, *14*, 1633.
[9] Y. Kuwabara, H. Ogawa, H. Inada, N. Noma, Y. Shirota, *Adv. Mater.* **1994**, *6*, 677.
[10] K. R. J. Thomas, J. T. Lin, Y. T. Tao, C. W. Ko, *J. Am. Chem. Soc.* **2001**, *123*, 9404.

ADVANCED MATERIALS

[11] V. Adamovich, J. Brooks, A. Tamayo, A. M. Alexander, P. I. Djurovich, M. E. Thompson, C. Adachi, B. W. D'Andrade, S. R. Forrest, *New J. Chem.* **2002**, *26*, 1171.
[12] M. A. Baldo, S. R. Forrest, *Phys. Rev. B* **2000**, *62*, 10 958.
[13] S. Lamansky, P. Djurovich, D. Murphy, F. Abdel-Razzaq, R. Kwong, I. Tsyba, M. Bortz, B. Mui, R. Bau, M. E. Thompson, *Inorg. Chem.* **2001**, *40*, 1704.
[14] V. Bulovic, V. B. Khalfin, G. Gu, P. E. Burrows, D. Z. Garbuzov, S. R. Forrest, *Phys. Rev. B* **1998**, *58*, 3730.
[15] M. H. Lu, J. C. Sturm, *J. Appl. Phys.* **2002**, *91*, 595.
[16] *Lighting Handbook*, IESNA, New York **1993**.
[17] B. D'Andrade, J. Brooks, V. Adamovich, M. E. Thompson, S. R. Forrest, *Adv. Mater.* **2002**, *14*, 1032.
[18] B. D'Andrade, M. E. Thompson, S. R. Forrest, *Adv. Mater.* **2002**, *14*, 147.
[19] G. Gu, V. Khalfin, S. R. Forrest, *Appl. Phys. Lett.* **1998**, *73*, 2399.
[20] G. B. Sabine, *Phys. Rev.* **1939**, *55*, 1064.
[21] G. Gu, D. Z. Garbuzov, P. E. Burrows, S. Venkatesh, S. R. Forrest, M. E. Thompson, *Opt. Lett.* **1997**, *22*, 396.
[22] I. G. Hill, A. Kahn, *J. Appl. Phys.* **1999**, *86*, 4515.
[23] C. W. Ko, Y. T. Tao, *Appl. Phys. Lett.* **2001**, *79*, 4234.
[24] X. Y. Jiang, Z. L. Zhang, W. M. Zhao, W. Q. Zhu, B. X. Zhang, S. H. Xu, *J. Phys. D* **2000**, *33*, 473.
[25] S. Y. Liu, J. S. Huang, Z. Y. Xie, Y. Wang, B. J. Chen, *Thin Solid Films* **2000**, *363*, 294.
[26] R. S. Deshpande, V. Bulovic, S. R. Forrest, *Appl. Phys. Lett.* **1999**, *75*, 888.
[27] F. Hide, P. Kozodoy, S. P. DenBaars, A. J. Heeger, *Appl. Phys. Lett.* **1997**, *70*, 2664.
[28] R. H. Jordan, A. Dodabalapur, M. Strukelj, T. M. Miller, *Appl. Phys. Lett.* **1996**, *68*, 1192.
[29] J. Kido, K. Hongawa, K. Okuyama, K. Nagai, *Appl. Phys. Lett.* **1994**, *64*, 815.
[30] M. H. Lu, M. S. Weaver, T. X. Zhou, M. Rothman, R. C. Kwong, M. Hack, J. J. Brown, *Appl. Phys. Lett.* **2002**, *81*, 3921.
[31] Y. J. Lee, S. H. Kim, J. Huh, G. H. Kim, Y. H. Lee, *Appl. Phys. Lett.* **2003**, *82*, 3779.
[32] S. Moller, S. R. Forrest, *J. Appl. Phys.* **2002**, *91*, 3324.
[33] T. Tsutsui, M. Yahiro, H. Yokogawa, K. Kawano, *Adv. Mater.* **2001**, *13*, 1149.

Nanoscale Surface Patterning of Enzyme-Catalyzed Polymeric Conducting Wires**

By *Peng Xu* and *David L. Kaplan**

Dip-pen nanolithography (DPN) technology has developed as a powerful tool for surface patterning at the nanometer scale. In the present study, 4-aminothiophenol, which can be coupled to gold, was used as "ink" for DPN patterning. The aim of the study was to combine enzymatic polymerization with DPN patterned reactive monomers to explore ambient surface reactions for the formation of conducting polymers. The products of these surface polymerization reactions were characterized by matrix-assisted laser desorption ionization time-of-flight (MALDI–TOF) mass spectrometry, X-ray photoelectron spectroscopy (XPS), and electrostatic force microscopy (EFM). The formation of nanowires using this modification of the DPN technique provides new opportunities for the formation of electrical contacts among structures, including biological components. This strategy suggests new directions in the fabrication and integration of synthetic and biological systems at the nanoscale.

There has been tremendous interest in the use of conducting polymers in various technology applications because of their electrical and optical properties, as well as their reasonable environmental stability.[1] Polyaniline and its derivatives are good candidates for conducting polymers, due to their conjugated atomistic structure and conjugation length. The common methods used to synthesize polyaniline and its derivatives are either electrochemical or chemical.[2–4] In both instances, methodologies are not biocompatible due to the harsh chemical or electrochemical conditions employed during polymer synthesis. Alternatively, enzymatic HRP-catalyzed (HRP: horseradish peroxidase) free-radical polymerization has been developed for the synthesis of conducting polymers.[5] As a biotechnological methodology, this approach has attracted attention due to its environmental compatibility, mild reaction conditions, high yields,[6,7] and water-soluble reactants.[8,9] Many efforts have been made to develop this method through manipulation of the reaction media or templates.[10–19] Mechanistic insight has also been reported.[20,21] The resultant polymers, such as polyaniline, are electrically conductive.[1] Conducting polymers are important materials in photovoltaics, solar cells, and molecular electronics. Many efforts are aimed at designing and manufacturing nanoscale devices including nanowires, nanonetworks, and nanotubes. Compared to metal, carbon, and semiconducting materials, polyaniline and related polymers may provide alternative, more flexible, nanodevices. They can be obtained either by in situ polymerization[2] or by self-assembly in solution.[3] Most polyaniline is synthesized and processed electrochemically.[22–24]

Two methods can be considered to pattern conducting polymers on surfaces. Synthesis of polymers in solution followed by direct surface patterning, or patterning monomers on surfaces followed by polymerization in situ. Direct DPN technology has been developed to deliver collections of molecules in a positive printing mode,[25] forming well-organized patterns of monomers and polymers at a nanometer scale. The surface organization is driven by self-assembly through ionic or covalent bonds or van der Waals' interactions.[26] Efforts have focused on the ink, the pen, the substrate, and the process.[26–34] Materials often used as the ink for DPN include alkyl thiols and thiolated biomolecules,[35,36] which can form covalent

[*] Prof. D. L. Kaplan, P. Xu
Departments of Biomedical Engineering and
Chemical and Biological Engineering
Bioengineering Center, Tufts University
4 Colby Street, Room 153, Medford, MA 02155 (USA)
E-mail: david.kaplan@tufts.edu

[**] Support from the Air Force MURI program is gratefully acknowledged. Technical assistance from D. Wilson and A. Singh (Tufts University) is gratefully acknowledged.

  DOI: 10.1002/adma.200306367